Variations of electron density based on long-term incoherent scatter radar and ionosonde measurements over Millstone Hill

Jiuhou Lei,[1,2] Libo Liu, and Weixing Wan

Institute of Geology and Geophysics, Chinese Academy of Sciences, Beijing, China

Shun-Rong Zhang

Haystack Observatory, Massachusetts Institute of Technology, Westford, Massachusetts, USA

Received 4 June 2004; revised 7 January 2005; accepted 9 February 2005; published 30 April 2005.

[1] Measurements from the incoherent scatter radar (ISR) and ionosonde over Millstone Hill (42.6°N, 288.5°E) are analyzed to explore ionospheric temporal variations. The F_2 layer peak density N_mF_2, peak height h_mF_2, and scale height H are derived from a Chapman α layer fitting to observed ISR electron density profiles. Diurnal, seasonal, and solar activity variations of the ionospheric characteristics are presented. Our study on the solar activity dependence of N_mF_2, h_mF_2, and H indicates that the peak parameters (N_mF_2 and h_mF_2) of the F_2 layer increase with daily $F_{10.7}$ index and saturate (or increase with a much lower rate) for very high $F_{10.7}$; however, they show almost linear dependence with the solar proxy index $F_{10.7p} = (F_{10.7} + F_{10.7A})/2$, where $F_{10.7A}$ is the 81-day running mean of daily $F_{10.7}$. This suggests that the overall effect of solar EUV and neutral atmosphere changes on the solar activity variation of ionospheric ionization is linear with $F_{10.7p}$. The rate of change in the ionospheric characteristics with solar activity exhibits a seasonal and local time variation. Over Millstone Hill, N_mF_2 in summer is characterized by the evening peak in its diurnal variation, and N_mF_2 exhibits winter anomaly under low and high solar activity levels. The temporal variations of the topside effective scale height H_0 can be explained in terms of those in the slab thickness. The IRI model overestimates the N_e effective topside scale height over Millstone Hill; therefore our analysis for the effective topside scale height from the Millstone Hill measurements might help to improve the IRI topside profiles at middle latitudes.

Citation: Lei, J., L. Liu, W. Wan, and S.-R. Zhang (2005), Variations of electron density based on long-term incoherent scatter radar and ionosonde measurements over Millstone Hill, *Radio Sci.*, *40*, RS2008, doi:10.1029/2004RS003106.

1. Introduction

[2] Knowledge of the ionospheric F_2 peak density N_mF_2, its peak height h_mF_2, or in some cases the whole electron density profile $N_e(h)$, is of great importance for ionospheric forecasting and ionospheric propagation studies. The ionospheric characteristics exhibit significant variations with solar cycle, season and local time, etc., which results from changes in the solar extreme ultraviolet (EUV) and X-ray radiations, and from various chemical and dynamic processes [e.g., *Balan et al.*, 1994a, 1994b; *Evans*, 1965; *Kane*, 1992; *Kawamura et al.*, 2002; *Richards et al.*, 1994b; *Richards*, 2001]. Therefore studies on the variations of these ionospheric characteristics are essential for ionospheric prediction and for understanding the physical mechanisms involved.

[3] Incoherent scatter radar (ISR) is by far the most powerful ground-based remote-probing tool for the study of the ionospheric processes. Since the 1960s, ISR measurements of electron density, plasma temperatures and line-of-sight ion drifts have been acquired over Millstone Hill, a favorable location at subauroral latitudes [*Holt et al.*, 2002]. Extensive data of ISR observations over Millstone Hill has enabled us to examine the temporal variations of important ionospheric parameters,

[1] Also at Wuhan Institute of Physics and Mathematics, Chinese Academy of Sciences, Wuhan, China.

[2] Also at Graduate School of Chinese Academy of Sciences, Beijing, China.

0048-6604/05/2004RS003106$11.00

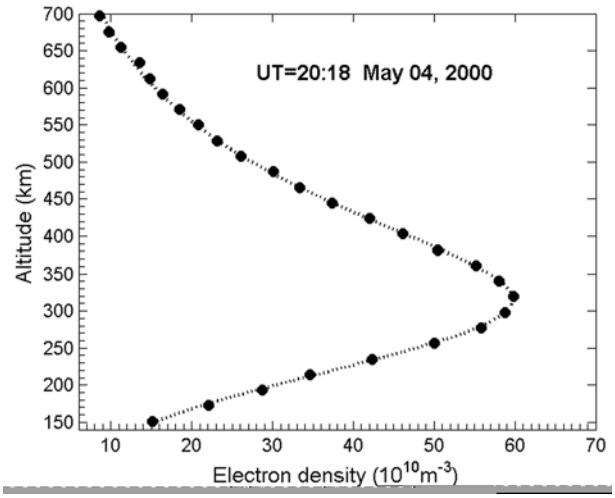

Figure 1. Comparison of the observed ISR electron density profile (solid circles) on 4 May 2000, with the fitted profile (dotted line) using the Chapman layer function.

such as the peak parameters (N_mF_2, h_mF_2) of F_2 layer and Chapman scale height H, which can be used to characterize the electron density profiles.

[4] The objective of the present study is to explore the temporal variations of the electron density based on the ISR data over Millstone Hill (42.6°N, 288.5°E), which covers more than two full solar cycles (1976–2002). We employ a Chapman layer to fit the observed ISR profiles and derive the ionospheric characteristics N_mF_2, h_mF_2, and H. The ionosonde measurements for the period 1989–1990 and 1998–2004 over Millstone Hill are also included to enlarge the database of the peak parameters N_mF_2 and h_mF_2. We present a comprehensive picture of the diurnal, seasonal and solar activity variations of these ionospheric characteristics.

2. Data Set and Analysis Method

[5] The Millstone Hill UHF ISR system operates with a zenith-directed 68 m fixed parabolic antenna, which commenced operation in 1963, and a fully steerable 46 m antenna, which commenced operation in 1978. More details about the ISR experiments and the data at Millstone Hill can be seen in the work of *Holt et al.* [2002]. The archived data are downloaded from the Madrigal online database system (http://www.openmadrigal.org) hosted by Millstone Hill Observatory. For this study measurements with pulse length >640 μs are excluded. Most of the remaining data have pulse length 300 μs or less with a height spacing of better than 22 km. The ISR data has been grouped into four seasonal bins of equal length centered on solstice and equinox days under low ($F_{10.7A} < 100$) and high ($F_{10.7A} > 150$) solar activity, respectively. The effects of geomagnetic activity are minimized by selecting data with 3-hourly $ap < 20$.

[6] To improve the statistics, we also include the ionosonde observations over Millstone Hill for the period 1989–1990 and 1998–2004 to get the F_2 layer peak parameters N_mF_2 and h_mF_2 with 3-hourly $ap < 20$. h_mF_2 was deduced from the empirical relationship among daily values of $M3000$, f_oF_2 and f_oE, as proposed by *Dudeney* [1983]. When f_oE was not available, it was calculated with a modified version of the CCIR formula [*Buonsanto and Titheridge*, 1987]. The same grouping process is performed for the ionosonde data as for the ISR measurements.

3. Results and Discussion

[7] Ionospheric characteristics are obtained from a fitting of ISR N_e profiles to a Chapman-α layer [*Rishbeth and Garriott*, 1969]:

$$N_e(h) = N_mF_2 \exp[0.5(1 - z - e^{-z})],$$
$$z = (h - h_mF_2)/H(h). \quad (1)$$

Since a two layer model can describe well electron density profiles within 150–600 km height range [*Fox*, 1994], we take Chapman scale height to be $H(h) = A_1 (h - h_mF_2) + H_m$ in the bottomside and $H(h) = A_2 (h - h_mF_2) + H_m$ in the topside. Thus N_mF_2, h_mF_2, H_m, A_1, and A_2 are adjustable variables, and can be determined by using the least squares fitting approach. This brings in the best match with the observed electron density profiles $N_e(h)$ [see *Lei et al.*, 2004].

[8] Our Chapman layer formalism is flexible and can be adjusted easily to generate a good representation to the observed N_e profile. Figure 1 shows an example of comparison between the original data profile and the fitted Chapman layer profile. Good agreement between the two profiles can be seen here, and in fact it prevails in most cases. Deviations become evident only under some conditions, such as during ionospheric storms which are not considered in this paper, when the ISR profile looks to be seriously distorted.

3.1. N_mF_2 Morphology

[9] Figure 2 shows the diurnal and seasonal variation of N_mF_2 under low and high solar activities. For low solar activity, after a sharp increase starting from 0600 LT, N_mF_2 in winter reaches its diurnal peak at 1300 LT. We note that there is a slight decrease during 0500–0600 LT. Compared to the high peak density in winter, the maximum N_mF_2 in spring becomes smaller at 1200–1300 LT; and the noon N_mF_2 in summer is lower by more than a factor of 2. It is interesting that the diurnal variation of N_mF_2 in summer can be characte-

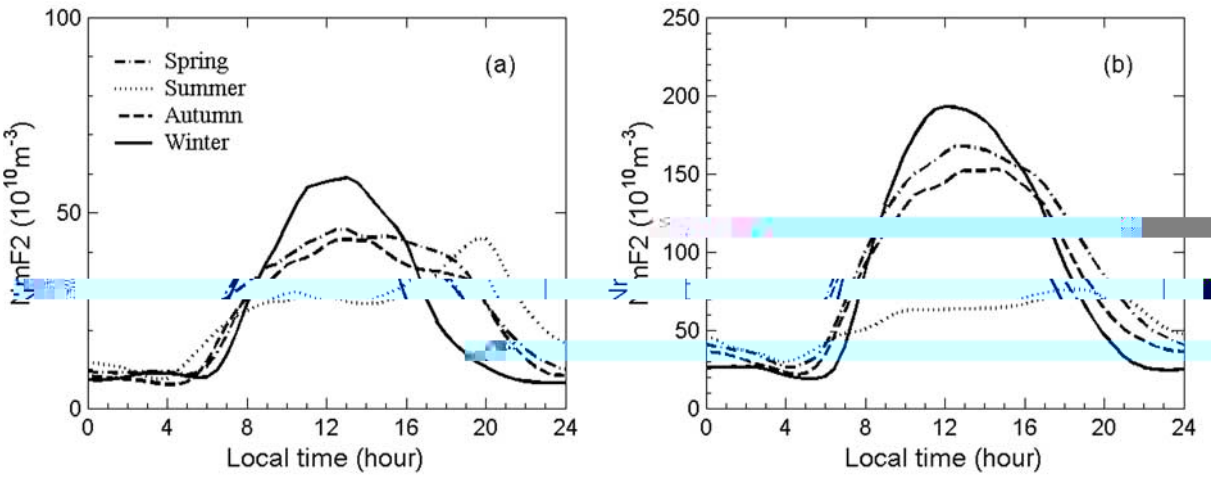

Figure 2. Diurnal and seasonal variation of the peak electron density (N_mF_2) under (a) low and (b) high solar activities.

rized by the evening (~2000 LT) peak. The evening enhancement in summer was considered to be associated with the large fall in the electron temperature [*Evans*, 1965] and the directional reverse of the meridional neutral wind [see *Eccles and Burge*, 1973]. The variation of N_mF_2 in autumn is intermediate between spring and summer, and the spring N_mF_2 is basically larger than the autumn one. Overall, the daytime N_mF_2 is highest in winter and lowest in summer, while the nighttime one shows the opposite tendency. The higher daytime density in winter than in summer is a manifestation of the well-known winter anomaly, which is mainly explained by the O/N_2 effect [*Rishbeth and Setty*, 1961], and partly by the effect of the vibrationally excited N_2 and O_2 [e.g., *Richards and Torr*, 1986; *Pavlov*, 1998]. For high solar activity, the diurnal and seasonal variations are generally similar to those under low solar activity, but they have considerable difference in detail. The winter anomaly is also pronounced and the daytime densities in winter become much larger, however, the evening peak in summer tends to be relatively weaker.

[10] With regard to the solar activity dependence, *Balan et al.* [1993, 1994a, 1994b] have shown that the ionospheric electron content (*IEC*) increases with increasing daily $F_{10.7}$ index and when $F_{10.7}$ exceeds a threshold (~160–200) it starts to saturate (remain constant). Through data and model calculations, *Balan et al.* [1993, 1994a, 1994b] interpreted the saturation in terms of the nonlinear relationship between the shorter wavelength solar fluxes that produce the ionosphere and the daily $F_{10.7}$ cm solar flux that has inappropriately been used as an index of solar activity. However, *Richards et al.* [1994b] reported that the measured N_mF_2 at Millstone Hill and Hobart are almost independent of daily $F_{10.7}$ index at solar maximum in 1990. *Richards* [2001] found that the solar cycle variation of ionosphere results from an almost equal increase in solar EUV ionizing flux and neutral atmosphere changes. Therefore electron density increases with solar activity in a complicated way, which can't be explained solely by the solar flux variations. Our long-term database provides a unique opportunity to study the solar activity variation of ionospheric ionization.

[11] Figure 3a shows the relationship of observed N_mF_2 to daily $F_{10.7}$ index at 1200 LT in winter. The fitted curve represents the average ionosphere while any deviation from it is due to day-to-day variability caused by gravity waves, changes in neutral densities and winds, fluctuations in the solar EUV flux, and the possible effect of magnetic activity. As can be seen, the N_mF_2 increases with daily $F_{10.7}$ when daily $F_{10.7}$ is less than 200, and then it remains almost constant when daily $F_{10.7}$ is greater than 200. This feature is consistent with previous studies of the dependence on daily $F_{10.7}$ for *IEC* [*Balan et al.*, 1993, 1994a, 1994b] and N_mF_2 [*Richards*, 2001]. Although the daily $F_{10.7}$ index has often been used as a proxy for solar EUV flux in ionospheric correlation studies, it is well known that it is not appropriate to use just the daily $F_{10.7}$ index. As mentioned earlier, *Richards et al.* [1994b] found that daytime N_mF_2 is almost independent of daily $F_{10.7}$ in summer at solar maximum at Millstone Hill and Hobart. *Hinteregger et al.* [1981] showed that the observed solar EUV fluxes could be well parameterized by linear combinations of the daily and 81 day average $F_{10.7}$ indices. *Richards et al.* [1994a] have shown that the solar cycle variation of most solar EUV flux lines can be scaled accurately enough for aeronomic applications by using $F_{10.7p} = (F_{10.7} + F_{10.7A})/2$ where

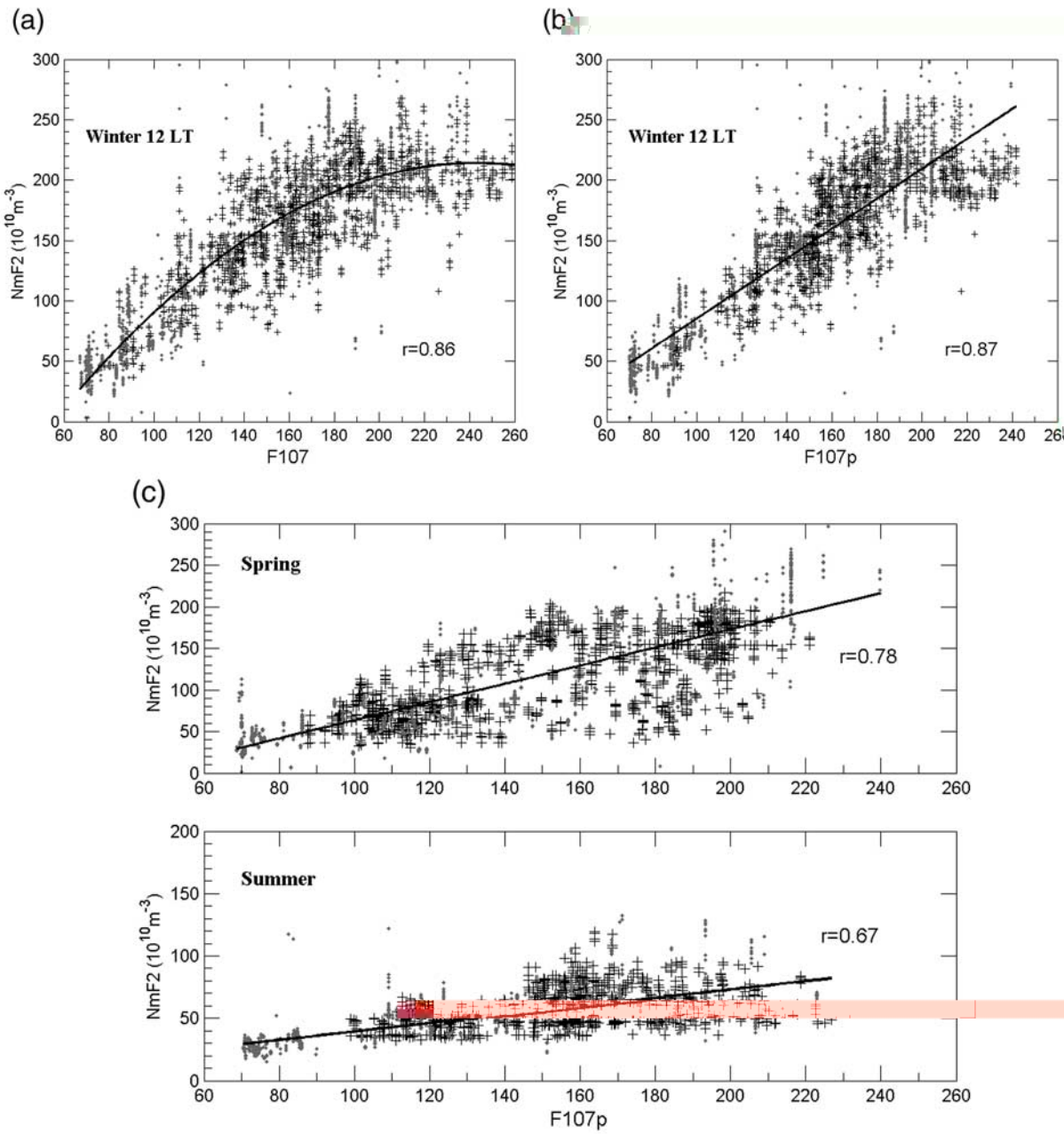

Figure 3. (a) The responses of the noon N_mF_2 to daily $F_{10.7}$ index; the observed data include those for ISR (points) and ionosonde (plus signs) measurements. The solid line is the results of a 2nd degree polynomial fitting for both type data, and r represents the correlation coefficient. (b) Same as Figure 3a, but for the responses of observed N_mF_2 to $F_{10.7p}$ index, and the solid line is

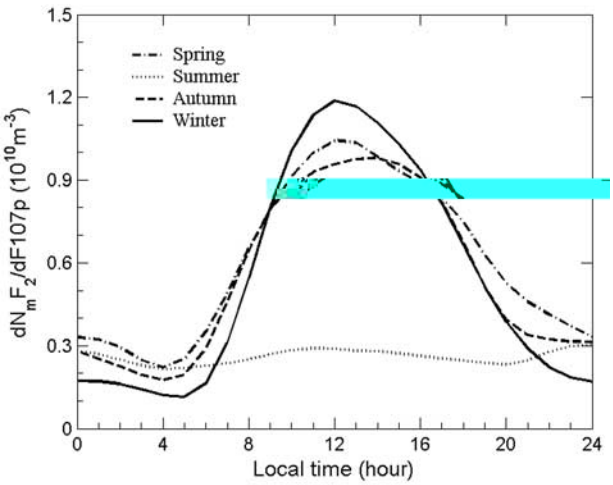

Figure 4. The diurnal variations of the gradient $dN_mF_2/dF_{10.7p}$, defined as the slope of the straight line for linear regression.

$F_{10.7A}$ is the 81-day running mean of daily $F_{10.7}$. Now we examine the winter N_mF_2 response to $F_{10.7p}$, as shown in Figure 3b. It can be seen that N_mF_2 increases linearly with increasing solar activity index $F_{10.7p}$ and a linear function can be used to represent the N_mF_2 and $F_{10.7p}$ correlation. Figure 3c shows the noon N_mF_2 as a function of $F_{10.7p}$ in spring and summer. We also can see that N_mF_2 shows almost linear dependence with $F_{10.7p}$ except for a little weaker correlation with solar activity. *Richards* [2001] showed that both EUV flux and neutral density changes are required to account for the full solar cycle variation of N_mF_2. The results in Figure 3 indicate that the overall effect of the EUV and neutral density changes is linear with respect to $F_{10.7p}$.

[12] Figure 4 displays diurnal variations of the gradient $dN_mF_2/dF_{10.7p}$, which are obtained with a linear regression. The slope or rate of change with respect to solar activity is larger during daytime and lower during nighttime except in summer when there is no difference in the gradient over the whole day. The seasonal variation of the midday gradient (or the increase rate) depends on the electron density values (see Figure 2), i.e., larger in winter, and smaller in summer. This is consistent with the findings of *Prasad and Rama Rao* [1993] and *Gupta and Singh* [2001] that the minimum and maximum gradients of IEC_{max} (daytime maximum value of *IEC*, one per day) versus solar flux just take place in the seasons of minimum and maximum *IEC*, respectively.

3.2. The h_mF_2 Morphology

[13] For low solar activity, as can be seen from Figure 5, h_mF_2 in winter shows two daytime minima at 0800 and 1600 LT. It reaches a diurnal minimum height of 230 km at 0800 LT, and a diurnal peak of 310 km at midnight. The h_mF_2 in equinoxes varies in a similar way to that in winter, but generally with relatively higher values by 10–20 km in autumn except for the sunrise period (0400–0800 LT). The variation of the summertime h_mF_2 exhibits a parabolic shape, with a relatively higher height by ~10 km during 1400–0400 LT than that in winter. Besides, h_mF_2 in summer decreases more markedly in the sunrise period than in other seasons. For high solar activity, although h_mF_2 is almost identical to that under low solar activity in the general trend of diurnal variation, it is higher by 50–70 km. Generally, the variations of h_mF_2 at middle latitudes can be explained in terms of the neutral winds and changes of the chemical compositions. The maximum h_mF_2 around midnight is caused by an increase of upward drifts produced by meridional winds [*Kohl and King*, 1967], while during the sunrise period, with the beginning of intensive photoionization, the layer maximum drops due to rapid production of ionization in the lower *F* region. We would expect a higher h_mF_2 in summer than winter because thermal expansion h_mF_2 should increase with increasing solar activity [*Rishbeth and Garriott*, 1969].

[14] h_mF_2 should increase with increasing solar activity [*Su et al.*, 1999; *Richards*, 2001]. We also find that measured h_mF_2 increases nonlinearly with daily $F_{10.7}$ while increases linearly with solar proxy $F_{10.7p}$, but for the sake of brevity we don't show the comparison of the solar activity variation of h_mF_2 with $F_{10.7}$ and $F_{10.7p}$ as Figure 3. Figure 6 demonstrates the diurnal variations of the slope $dh_mF_2/dF_{10.7p}$ generally with higher values

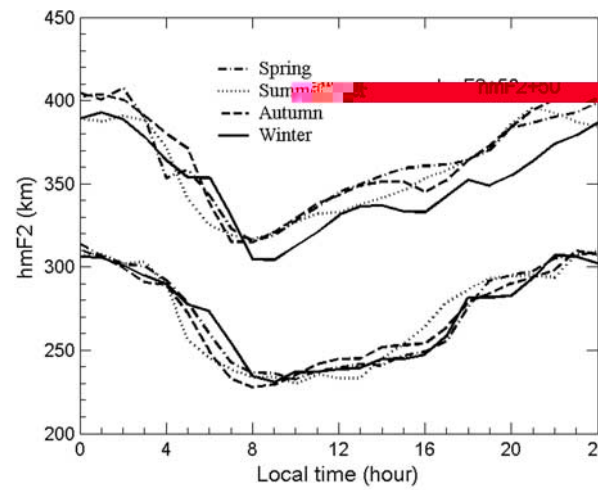

Figure 5. Diurnal and seasonal variation of the peak heights (h_mF_2) under low (lower four curves) and high (upper four curves, shifted by +50 km) solar activities.

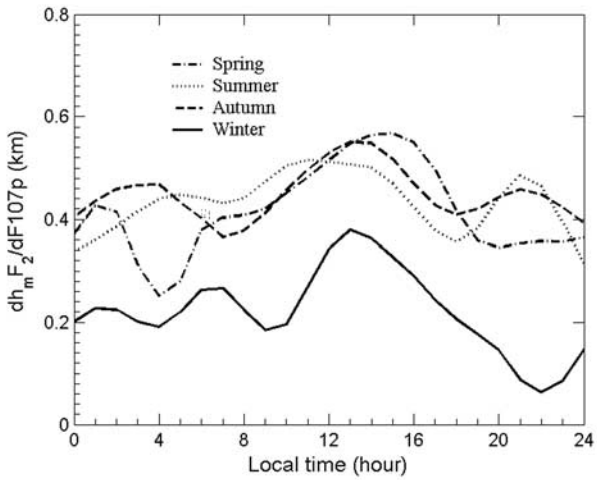

Figure 6. Same as Figure 4, but for $dh_mF_2/dF_{10.7p}$.

during daytime than at night, and with a diurnal peak at around 1300–1400 LT in all seasons. It is interesting to note that this rate of change is also positively correlated with the h_mF_2 values, with both the rate and h_mF_2 lower in winter than in other seasons. This solar activity variation of h_mF_2 is mainly attributed to the corresponding variation of the neutral temperature and neutral concentrations that control the chemical loss and diffusion balance height and the height of the peak production [see *Zhang et al.*, 1999].

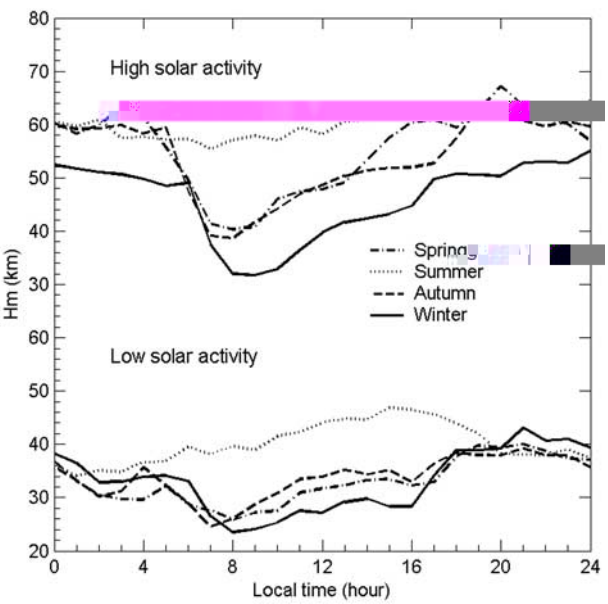

Figure 7. Diurnal and seasonal variations of scale heights (H_m) under low and high solar activities.

3.3. Chapman Scale Height *H*

[15] A Chapman-type layer is predicted by a simplified aeronomic theory, assuming photoionization in a one-species neutral gas, and neglecting transport processes [*Rishbeth and Garriott*, 1969]. Note that the Chapman layer is a fitting device and does not represent actual physics of the *F* layer ionosphere because a Chapman process does not form the F_2 layer. The determined *H* becomes an effective scale height because of the possible influence of transport processes and additional neutral species.

[16] Figure 7 presents diurnal and seasonal variations of the scale height H_m, which somewhat reflects the effective scale height at h_mF_2. It is seen that the scale height H_m also undergoes appreciable changes with local time, season, and solar activity. For low solar activity, H_m decreases from night to day in winter and equinoxes, whereas it increases from night to day in summer. The minimum values of H_m occur at 0700 LT in equinoxes and 0800 LT in winter. It is found that daytime values are higher in summer and lower in winter with equinox in halfway between the two solstices; while nighttime values exhibit less seasonal variation. The value of H_m under high solar activity is generally higher by about 10–20 km as compared to that under low solar activity.

[17] Figure 8 illustrates responses of scale height H_m to solar activity. It is evident that H_m also displays a linear dependence on $F_{10.7p}$ as N_mF_2 and h_mF_2. The rate of change $d(H_m)/d(F_{10.7p})$, as shown in Figure 9, indicates a lower value during daytime, and the day-night difference of H_m increases with solar activity except for summer.

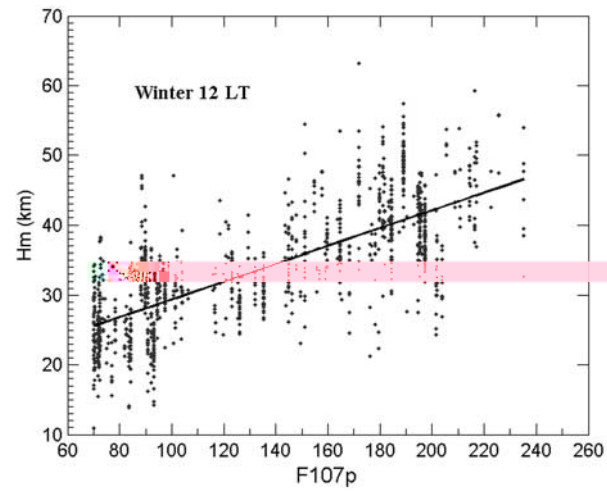

Figure 8. An example of the variation of scale height H_m with solar flux index $F_{10.7p}$. The solid line is the results from linear regression.

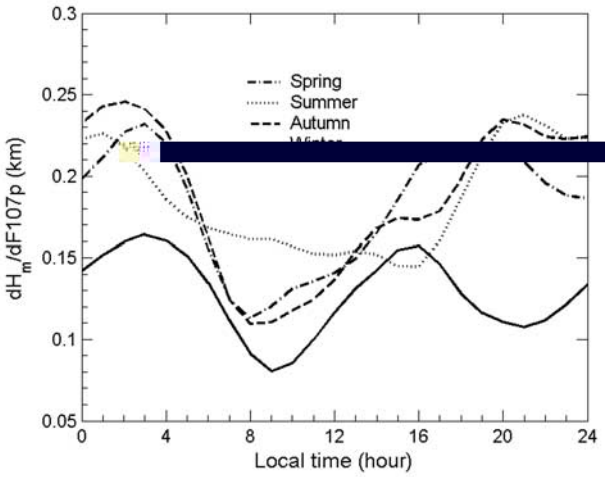

Figure 9. Same as Figure 4, but for the rate of change $d(H_m)/d(F_{10.7p})$.

The slopes are higher in equinoxes and summer than in winter. In addition, the parameter A_1 for the bottomside profile is always negative (>−0.3), implying the scale height being larger below the peak than at the peak. The nighttime values are generally larger than the daytime ones. For the topside parameter A_2, it varies from 0.02 to 0.1 and with two peaks occurring at predawn and sunset hours (not shown). Our statistical study demonstrates that the density profile for both bottomside and topside can be best fitted by the scale height H that increases with the absolute value of $h - h_mF_2$.

[18] As the scale height varies with height, it will be worthwhile to define an effective topside scale height H_0 which does not vary with height in order to quantify the general magnitude of change of N_e with height. For the α-Chapman layer with a variable scale height in equation (1), the topside electron content is

$$\Phi = \int_{h_mF_2}^{700} N_mF_2 \exp[0.5(1 - z - e^{-z})]dh,$$
$$z = \frac{h - h_mF_2}{A_2(h - h_mF_2) + H_m}, \quad (2)$$

where we ignore contributions from above 700 km [*Huang and Reinisch*, 2001]. For H_0, the density at a given height is

$$N_e(h) = N_mF_2 \exp\left\{0.5\left[1 - \frac{h - h_mF_2}{H_0} - \exp\left(-\frac{h - h_mF_2}{H_0}\right)\right]\right\}, \quad (3)$$

and its integral giving the topside electron content is as follows:

$$\Phi = \int_{h_mF_2}^{\infty} N_e(h)dh \approx 2.82H_0N_mF_2. \quad (4)$$

Then, the constant effective scale height H_0 is obtained in the following integration,

$$H_0 \approx \frac{1}{2.82} \int_{h_mF_2}^{700} \exp[0.5(1 - z - e^{-z})]dh,$$
$$z = \frac{h - h_mF_2}{A_2(h - h_mF_2) + H_m}. \quad (5)$$

Now that a variable scale height has been adopted, the scale height H_m cannot be equal to the topside effective scale height H_0. As shown in Figure 10, H_0 shares a similar tendency with H_m except that the values of H_0 are generally higher by ~10–15 km and the day-to-night difference in summer becomes larger.

[19] Variations of H_0 show excellent agreement with that of slab thickness τ (τ = TEC/N_mF_2) as reported by *Titheridge* [1973] and *Davies and Liu* [1991], and this is due to a good positive correlation between the slab thickness and the topside effective scale height [*Huang and Reinisch*, 2001]. It seems to us that the diurnal variation exhibits a predawn increase, with varying onset

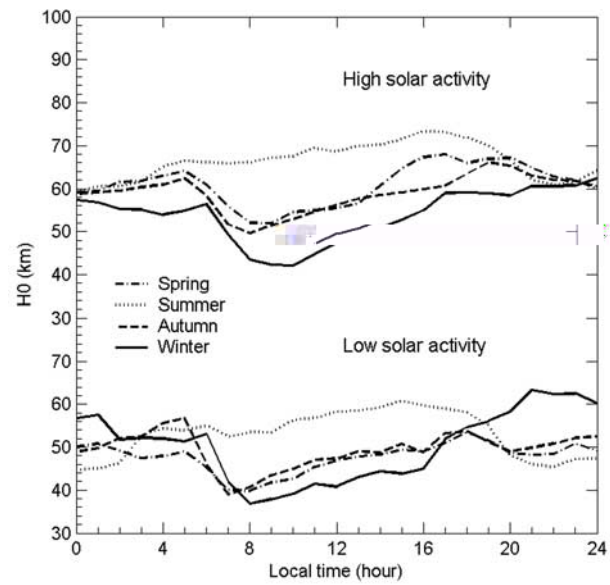

Figure 10. Diurnal and seasonal variations of effective topside scale heights H_0 under low and high solar activities.

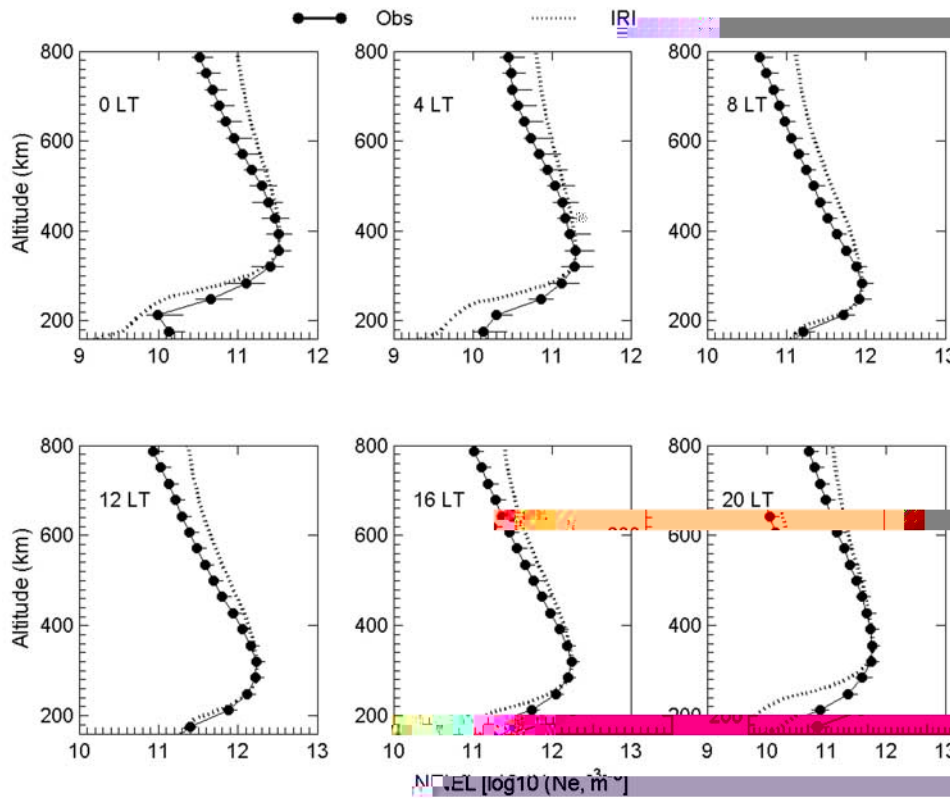

Figure 11. Comparisons of hourly N_e profiles from a monthlong ISR observations (October 2002) over Millstone Hill with the IRI2001 model. The horizontal bars cover the lower quartile through median values to the upper quartile.

time from 0500 LT in equinox to 0600 LT in winter. The timing corresponds to that of low values of N_mF_2 (see Figure 2) which are attributed to a downward movement of the ionosphere when the neutral winds decrease or reverse, and the increased loss rate at lower heights from 0500 to 0600 LT causes a more severe decay at peak height than at other heights, making the F_2 region N_e profile flat in shape. During 0800–1600 LT H_0 shows an approximately linear increase (Figure 10), which may be associated with a steady increase in temperature. The higher nighttime H_0 in winter and equinox indicates that the electron density profiles are flatter reflecting a far more severe decay at the peak height than at other altitudes. Moreover, the larger nighttime H_0 in winter is probably a heating effect from the conjugate photoelectrons. Plasmaspheric fluxes and H^+ at nighttime may alter the topside scale height (see the analysis for slab thickness by *Titheridge* [1973]). The topside H_0 is a good measure of the plasma temperatures, since the topside ionosphere profile shape is mostly determined by the plasma diffusion. H_0 should be somehow related to the plasma scale height. Both T_i and T_e are higher in summer than in winter in the topside ionosphere, therefore giving rise to N_e decreasing more rapidly in winter than in summer, or smaller winter timescale height.

3.4. Discussion

[20] At low and middle latitudes, the primary source of ionization in the F region is the EUV solar irradiances. The solar activity dependence of ionospheric characteristics has been studied in the early various ionospheric observations. Several studies [e.g., *Kane*, 1992; *Rishbeth*, 1993; *Richards*, 2001] have shown that the linear relationship of the ionospheric ionization with $F_{10.7}$ breaks down for high values of $F_{10.7}$. *Balan et al.* [1993, 1994a, 1994b, 1996] have studied the responses of *IEC* to solar activity, and found that the ionospheric density increases nonlinearly with daily $F_{10.7}$ and that the nonlinear variations of ionospheric characteristics are caused by the nonlinear relationships with $F_{10.7}$ of the solar EUV fluxes. However, *Richards* [2001] found that the solar cycle variation of ionosphere can't be explained solely by the solar flux variations. Our results show that the observed N_mF_2 at Millstone Hill exhibits almost linear relationship

with the solar activity index $F_{10.7p}$ in all seasons (Figure 3), and suggest that the total effect of both solar EUV and neutral atmosphere changes on the solar activity variation of ionospheric ionization is linear with $F_{10.7p}$. The comparisons of measured and theoretical electron density as *Richards* [2001] did will help us in further understanding the seasonal and solar activity variations over Millstone Hill. This point deserves further investigation.

[21] However, recent studies showed that the IRI predictions present frequent disagreement with observations because the current IRI topside profile is largely based on a small set of ISIS topside profiles. For example, Figure 11 shows a comparison of monthly median N_e profiles from a monthlong ISR observations (October 2002) over Millstone Hill with the IRI2001 model. Note that the observed h_mF_2, N_mF_2 are used as input parameters of IRI2001 to compute the hourly N_e profiles. The $N_e(h)$ plots reveal that IRI model produces reasonably good results for the bottomside profiles during daytime, while it underestimates the bottomside profiles during nighttime, and significantly overestimates the topside profiles. A multiplicative correction factor (Ne_{obs}/Ne_{IRI}) at 800 km is $\sim$0.5 on average is applied to bring the model in agreement with the observed topside profiles. This factor generally agrees with that of *Bilitza* [2004]. Many efforts have been made on the improvement for the IRI topside electron density profile model [e.g., *Bilitza*, 2001, 2004; *Huang and Reinisch*, 2001]. *Huang and Reinisch* [2001] introduced a technique for calculating the vertical TEC from ground-based ionosonde measurements, assuming a constant scale height for the topside profile. Instead of using only the bottomside profile, we have derived the information about the effective scale height directly from the entire ISR electron density profile (see Figures 7–10). Therefore our analysis for the measurements over Millstone Hill might open up the possibility of improving the IRI topside profiles at middle latitudes.

[22] As discussed by *Fox* [1994], the Chapman function is simple and analytic, and has great potential for modeling ionospheric electron density height variation. On the basis of our long-term data study of basic ionospheric characteristics, we find it appropriate to use α layer function for representing the electron density height variation in a midlatitude N_e model

Balan, N., G. J. Bailey, and Y. Z. Su (1996), Variations of the ionosphere and related solar fluxes during solar cycles 21 and 22, *Adv. Space Res.*, *18*(3), 11–14.

Bilitza, D. (2001), International reference ionosphere 2000, *Radio Sci.*, *36*(2), 261–275.

Bilitza, D. (2004), A correction for the IRI topside electron density model based on Alouette/ISIS topside sounder data, *Adv. Space Res.*, *33*, 838–843, doi:10.1016/j.asr.2003.07.009.

Buonsanto, M. J., and J. E. Titheridge (1987), Diurnal variations in the flux of ionisation above the F_2 peak in the Northern and Southern Hemispheres, *J. Atoms. Terr. Phys.*, *49*, 1093–1105.

Davies, K., and X. M. Liu (1991), Ionospheric slab thickness in middle and low latitude, *Radio Sci.*, *26*(4), 997–1005.

Dudeney, J. R. (1983), The accuracy of simple methods for determining the height of the maximum electron concentration of the F_2 layer from scaled ionospheric characteristics, *J. Atmos. Terr. Phys.*, *45*, 629–640.

Eccles, D., and J. D. Burge (1973), The behavior of the upper ionosphere over North America at sunset, *J. Atmos. Terr. Phys.*, *35*, 1927–1934.

Evans, J. V. (1965), Cause of the mid-latitude evening increase in f_oF_2, *J. Geophys. Res.*, *70*(5), 1175–1185.

Fox, M. W. (1994), A simple, convenient formalism for electron density profiles, *Radio Sci.*, *29*(6), 1473–1491.

Gupta, J. K., and L. Singh (2001), Long term ionospheric electron content variations over Delhi, *Ann. Geophys.*, *18*, 1635–1644.

Hinteregger, H. E., K. Fukui, and B. R. Gilson (1981), Observational, reference, and model data on solar EUV from measurements on AE-E, *Geophys. Res. Lett.*, *8*, 1147–1150.

Holt, J. M., S. Zhang, and M. J. Buonsanto (2002), Regional and local ionospheric models based on Millstone Hill incoherent scatter radar data, *Geophys. Res. Lett.*, *29*(8), 1207, doi:10.1029/2002GL014678.

Huang, X., and B. W. Reinisch (2001), Vertical electron content from ionograms in real time, *Radio Sci.*, *36*(2), 335–342.

Kane, R. P. (1992), Sunspots, solar radio noise, solar EUV and ionospheric f_oF_2, *J. Atmos. Terr. Phys.*, *54*, 463–466.

Kawamura, S., N. Balan, Y. Otsuka, and S. Fukao (2002), Annual and semiannual variations of the midlatitude ionosphere under low solar activity, *J. Geophys. Res.*, *107*(A8), 1166, doi:10.1029/2001JA000267.

Kohl, H., and J. W. King (1967), Atmospheric winds between 100 and 700 km and their effects on the ionosphere, *J. Atmos. Terr. Phys.*, *29*, 1045–1062.

Lei, J., L. Liu, W. Wan, S. Zhang, and J. M. Holt (2004), A statistical study of ionospheric profile parameters derived from Millstone Hill incoherent scatter radar measurements, *Geophys. Res. Lett.*, *31*, L14804, doi:10.1029/2004GL020578.

Pavlov, A. V. (1998), The role of vibrationally excited oxygen and nitrogen in the ionosphere during the undisturbed and geomagnetic storm period of 6–12 April 1990, *Ann. Geophys.*, *16*, 589–601.

Prasad, D. S. V. V. D., and P. V. S. Rama Rao (1993), Day-to-day variability of ionospheric electron content over Waltair, *Ind. J. Radio Space Phys.*, *22*, 391–396.

Richards, P. G. (2001), Seasonal and solar cycle variations of the ionospheric peak electron density: Comparison of measurement and models, *J. Geophys. Res.*, *106*(A12), 12,803–12,819.

Richards, P. G., and D. G. Torr (1986), A factor of 2 reduction in theoretical F_2 peak electron density due to enhanced vibrational excitation of N_2 in summer at solar maximum, *J. Geophys. Res.*, *91*(A10), 11,331–11,336.

Richards, P. G., J. A. Fennelly, and D. G. Torr (1994a), EUVAC: A solar EUV flux model for aeronomic calculations, *J. Geophys. Res.*, *99*(A5), 8981–8992.

Richards, P. G., D. G. Torr, B. W. Reinisch, R. R. Gamache, and P. J. Wilkinson (1994b), F_2 peak electron density at Millstone Hill and Hobart: Comparison of theory and measurement at solar maximum, *J. Geophys. Res.*, *99*(A8), 15,005–15,016.

Rishbeth, H. (1993), Day-to day ionospheric variations in a period of high solar activity, *J. Atmos. Terr. Phys.*, *55*, 165–171.

Rishbeth, H., and O. K. Garriott (1969), *Introduction to Ionospheric Physics*, Elsevier, New York.

Rishbeth, H., and C. S. G. K. Setty (1961), The *F* layer at sunrise, *J. Atmos. Terr. Phys.*, *10*, 263–276.

Su, Y. Z., G. J. Bailey, and S. Fukao (1999), Altitude dependences in the solar activity variations of the ionospheric electron density, *J. Geophys. Res.*, *104*(A7), 14,879–14,891.

Titheridge, J. E. (1973), The slab thickness of the mid-latitude ionosphere, *Planet Space Sci.*, *21*, 1775–1793.

Zhang, S.-R., S. Fukao, W. L. Oliver, and Y. Otsuka (1999), The height of the maximum ionospheric electron density over the MU radar, *J. Atmos. Sol. Terr. Phys.*, *61*, 1367–1383.

J. Lei, L. Liu, and W. Wan, Institute of Geology and Geophysics, Chinese Academy of Sciences, Beijing 100029, China. (leijh@mail.igcas.ac.cn; liul@mail.igcas.ac.cn; wanw@mail.igcas.ac.cn)

S.-R. Zhang, Haystack Observatory, Massachusetts Institute of Technology, Route 40, Westford, MA 01886, USA. (shunrong@haystack.mit.edu)